Friction

Research Article

Friction behavior of graphene edges within a carbon surface

Kun Sun[1], Mingjun Sun[1], Ri Pan[1,✉], Meijie Yin[2,✉], Kai Qi[3], Dongju Chen[1], Jinwei Fan[1], Dongfeng Diao[2,✉]

Cite this article: Sun K, Sun MJ, Pan R, et al. *Friction* 2026, **14**(1): 9441086. https://doi.org/10.26599/FRICT.2025.9441086

ABSTRACT: We report the friction behavior of graphene edges within a carbon film, which encompasses structures ranging from amorphous carbon (a-C) to graphene nanocrystalline carbon (GNC). Structural characterization revealed that vertically growing graphene nanocrystallites were implanted into the a-C structure, exposing high-density layer edges on the film surface. Atomic force microscopy (AFM) nanofriction tests highlighted the nature of graphene edge friction. Firstly, the edge friction of GNC films was tested in a critical-contact state, and the results showed that graphene edges exhibited lower friction forces than did a-C edges. Secondly, the surface friction of GNC films was investigated in a full-contact state, revealing that the edge friction of graphene nanocrystallites regulated the surface friction of GNC films. As the edge density of graphene nanocrystallites increased, the nanofriction force of GNC films decreased. Finally, the mechanism of the regulated friction behavior was attributed to the number of edges of the graphene nanocrystallites, which provided plentiful sp^2 C dangling bonds with weak bonding interactions and edge quantum wells with low surface potentials for lowering friction. These findings shed light on the importance of graphene-related materials and their high-density edges in the structural design and nanofriction application of carbon films.

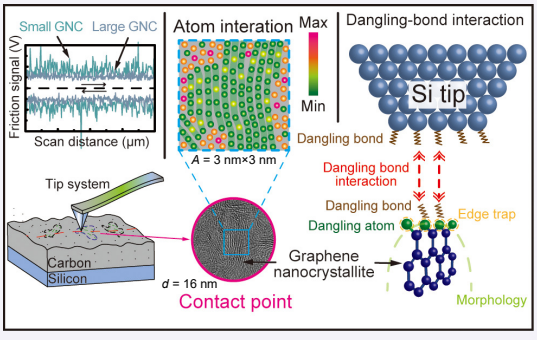

KEYWORDS: edge friction; graphene nanocrystallite; sp^2 C; carbon film; nanofriction

1 Introduction

With the rapid development of nanotechnology, emerging nano/micro devices have expanded human cognitive horizons and enhanced living experience [1–3]. In small-scale applications, friction forces play an important role in surface driving, terminal actuation, and contact protection for micro/nanosystems, such as nanoactuators, microgrids, and small robots [4–6]. Both scientific and industrial communities have attempted to determine the origin of friction to control the surface friction force [7–9]. However, controlling the nanofriction force is still challenging in probing and understanding the nature of surface friction.

Friction is a resistance process of contact and sliding surfaces. As two surfaces approach and contact, the atoms at the surface terminal play a crucial role in surface interactions, such as molecular forces (van der Waals forces), electrostatic forces, bonding forces, etc., and then, relative motion occurs at the two surfaces, and those surface interactions become resistance forces [10–12]. At the atomic scale, the friction force highly depends on surface interactions, which are regulated by individual atoms within surface structures [13–15]. However, complex surface structures always lead to unpredictable and uncontrollable friction forces.

Over the past few decades, numerous nanofriction studies have focused on graphene and related two-dimensional (2D) carbon materials (mainly composed of sp^2 hybridized C atoms) because of their perfect layer surfaces and potential nano/micro applications [16–18]. In those graphene-related surfaces, the in-plane layer structure provides weak van der Waals forces for low-friction behavior, and the layer surface wrinkles and structural defects control the friction state [19–21]. Among those studies, few have reported the edge friction behavior of graphene-related materials, especially the layer edges on the out-of-plane surface, due to scale restrictions. Recently, graphene edges and their defects have been reported to have an enhancement effect on electricity and show great potential in the application of electronic, photoelectric, electromagnetic, and other devices [22–24]. The investigation of the nanofriction behavior of graphene edges to support and develop applications is urgently needed. In recent work, we reported a graphene nanocrystallite carbon (GNC) film with a hybrid structure of vertically growing graphene nanocrystallite-implanted amorphous carbon (a-C) phases with high-density graphene edges exposed on the top surface [25]. This special surface structure provides a chance to probe the friction behavior of graphene edges. Additionally, a-C materials, as important 2D anti-friction coatings, often present incoherent surface states for

[1] Beijing Key Laboratory of Advanced Manufacturing Technology, College of Mechanical and Energy Engineering, Beijing University of Technology, Beijing 100124, China. [2] Institute of Nanosurface Science and Engineering (INSE), Shenzhen University, Shenzhen 518060, China. [3] Department of Chemical System Engineering, School of Engineering, the University of Tokyo, Tokyo 1130033, Japan.

✉ Corresponding authors. E-mail: R. Pan, panri@bjut.edu.cn; M. Yin, yinmj@szu.edu.cn; D. Diao, dfdiao@szu.edu.cn

Received: July 18, 2024; Revised: November 20, 2024; Accepted: February 27, 2025

predicting and controlling surface friction forces because of their complex components of sp^{2}- and sp^{3}-hybridized C atoms [26–28]. However, the GNC film has a regulated surface structure ranging from the a-C state to the GNC state for potential control of the nanofriction behavior. Therefore, a thorough investigation into the nanofriction behavior of GNC surfaces with structural evolution from a-C to GNC is of great significance in understanding the nature of edge friction.

In this study, a GNC film was obtained using an electron cyclotron resonance (ECR) plasma system. The structural evolution and friction behavior of high-density graphene edges within GNC surfaces were investigated. The friction force at the atomic scale can be controlled by the edges of graphene on the film surface. The corresponding mechanism was also discussed.

2 Structure of GNC film

Figure 1 shows the surface fabrication, structure, and morphology characterization of the GNC films. As shown in Fig. 1(a), a GNC film was deposited on a p-silicon wafer via low-energy electron irradiation, which was conducted in an ECR Ar plasma [25]. During the Ar plasma, a positive bias was applied to the deposited Si wafer fixed on the steel substrate to achieve electron irradiation. According to the electron irradiation energies of 20, 50, and 80 eV, different GNC films were obtained and defined as e+20, e+50, and e+80 samples, respectively. For comparison, an a-C film was obtained under ion irradiation mode with an irradiation energy of 10 eV (defined as the i–10 sample), which was conducted with a negative substrate bias. The cross-sectional structure of the GNC film was characterized by a transmission electron microscope (TEM; Titan Cubed Themis G2 300, FEI) along with a focused ion beam (FIB; Scios, FEI). In the cross-sectional TEM images (Fig. 1(a)), the low-magnification image of the electron irradiation film (e+50 sample) revealed that the film thickness was approximately 100 nm, and the high-magnification images of the middle zone (zone I) and bottom zone (zone II) revealed that some layer structures were regularly arranged into the amorphous phase and perpendicular to the Si wafer (this vertically growing mode is defined as "standing"). The interplanar spacing of the multilayer structure was approximately 0.36 nm, corresponding to the multilayer graphene phase. Essentially, the multilayer graphene arrangement belonged to one nanocrystalline structure. Thus, a GNC film with "standing" (vertically growing) graphene nanocrystallites was obtained through electron irradiation.

Figure 1(b) shows the surface structures of the a-C and GNC films, which were analyzed via top-view TEM observation and Raman spectra analysis. The ion irradiation film (i–10 sample) was amorphous without any discernible nanostructural features in the high-resolution TEM image, and the amorphous phase marked zone 1 presented a vague ring in the fast Fourier transform (FFT) image. The Raman spectrum of the i–10 a-C film displayed a single band at approximately 1,550 cm^{-1} and an absence of an obvious 2D band at approximately 2,700 cm^{-1}. In contrast, the electron irradiation films (e+20, e+50, and e+80 samples) all contained graphene nanocrystallites randomly distributed among the film structure and the graphene layer edges exposed on the top surface in the top-view TEM images. In the FFT images, the multilayer graphene phase (marked as zones 2, 4, and 6) and the amorphous phase (marked as zones 3, 5, and 7) presented two bright points and one vague ring, respectively, which suggested the presence of graphene nanocrystallites in the amorphous structure. The Raman spectra of the GNC films all displayed two independent D and G bands, located at approximately 1,350 and 1,580 cm^{-1}, respectively, along with a well-defined 2D band located at approximately 2,700 cm^{-1}. Typically, the D band and the G band, originating from the phonon resonance of defects or edges in nanocrystalline structures, are used to evaluate the state of graphene nanocrystallites, and the 2D band, originating from the two-phonon-involved double

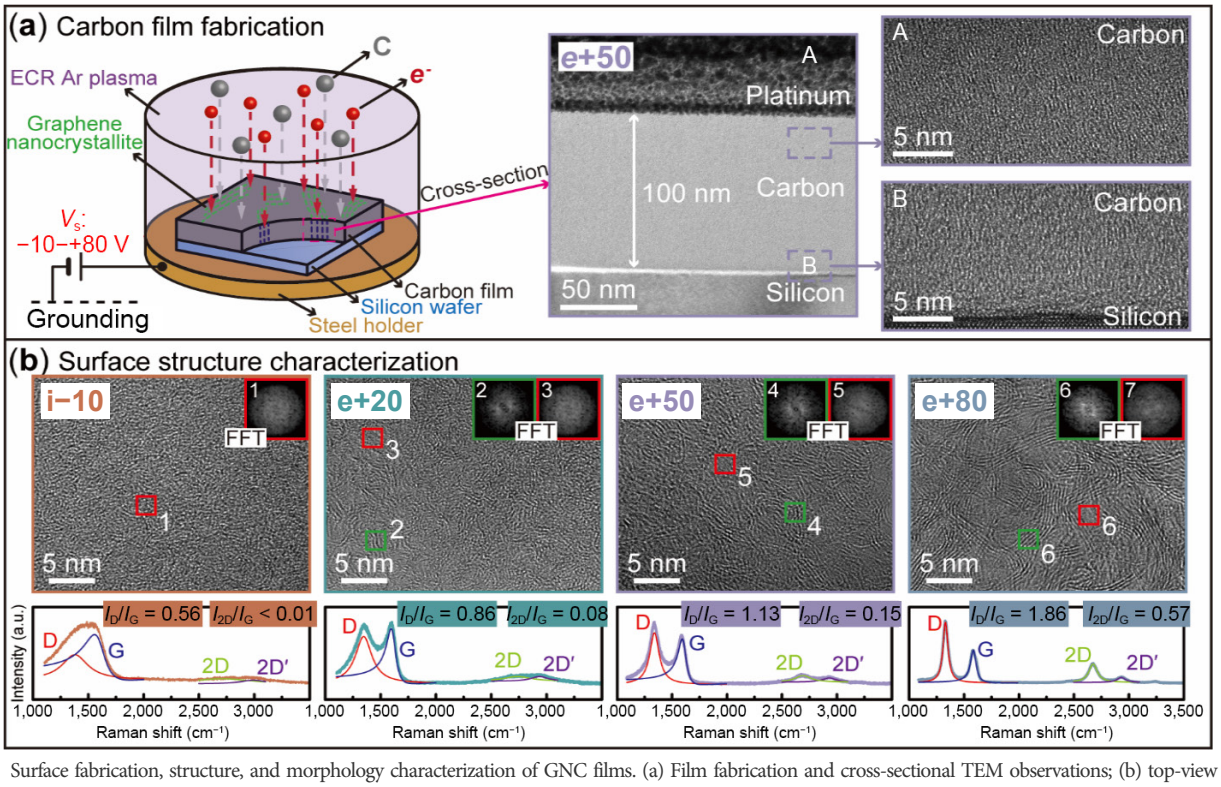

Fig. 1 Surface fabrication, structure, and morphology characterization of GNC films. (a) Film fabrication and cross-sectional TEM observations; (b) top-view TEM observations and Raman spectra analyses of different GNC films.

resonance between the graphene layers, is used to analyze multilayer graphene [29]. The clearly separated D and G bands, along with the obvious 2D band in the Raman spectra, confirmed that the GNC films were composed of one graphene nanocrystalline structure containing many structural defects and edges. Consequently, the GNC film was a coupling structure of "standing" graphene nanocrystallites implanted into the amorphous phase.

Compared with those of the GNC films, the graphene nanocrystalline state, as well as the edge structure, intensified with increasing electron irradiation energy. In the e+20 GNC film, the TEM image revealed that slight graphene nanocrystallites with many layer edges randomly appeared in the full-field view, and the nanocrystallite sizes were 1–2 nm, indicating that high-density edge structures began to form on the carbon surface. The Raman spectra revealed two divided D and G bands along with a vague 2D band, also indicating the initial presence of a graphene nanocrystalline structure in the carbon film. In the e+50 GNC film, the TEM image revealed that large-scale graphene nanocrystallites were distributed in an ordered manner, the nanocrystallite size increased to 3–5 nm, and the number of layers increased. The increased crystallinity of the graphene layer structures led to more high-density edges being exposed on the top surface. The increased D band density, decreased G band density, and distinct 2D band density in the Raman spectra indicated the presence of more graphene nanocrystallites in the carbon film. In the e+80 GNC film, the TEM image showed that long-range graphene nanocrystallites with high-density edges appeared in the carbon structure, with the nanocrystallite sizes enlarging to 8–15 nm and the layer numbers approaching 10. The high D and 2D bands in the Raman spectra indicated that the e+80 sample contained many high-density edges of graphene nanocrystallites on the carbon surface. In addition, the increased I_D/I_G value (intensity ratio of D and G bands) from 0.86 to 1.86 confirmed that more large-scale graphene nanocrystallites with abundant structural edges and defects formed in the GNC film, and the increased I_{2D}/I_G value (intensity ratio of 2D and G bands) from 0.08 to 1.57 suggested an increase in the number of graphene layers [30]. Thus, the states of graphene nanocrystallites and their high-density edges in the GNC film could be controlled by adjusting the electron irradiation energy.

3 Friction of graphene edge within GNC film

Figure 2 presents the friction behavior of the graphene edges within the GNC films. The friction behavior of the graphene edges was tested via an atomic force microscope (AFM; Dimension Icon, Bruker) equipped with a 16-nm-diameter silicon probe

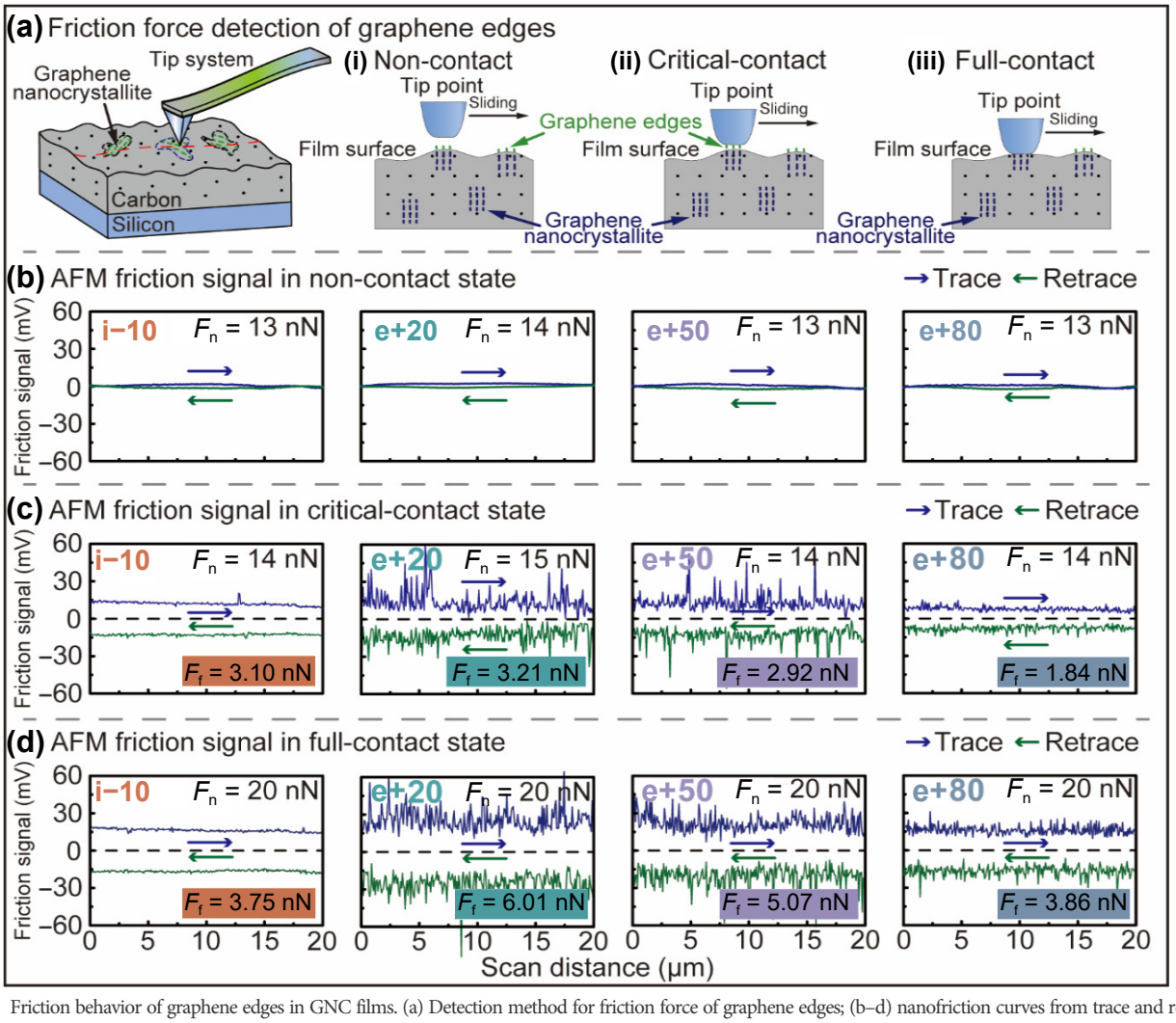

Fig. 2 Friction behavior of graphene edges in GNC films. (a) Detection method for friction force of graphene edges; (b–d) nanofriction curves from trace and retrace scans for noncontact, critical-contact, and full-contact states; scanning size was 20 μm × 20 μm, and scanning speed was 1 μm/s. Test temperature was 25±2 °C, and relative humidity was 20%–30%.

清華大学出版社 Tsinghua University Press | SciOpen

(CONTV-A) operating in contact mode at a scan frequency of 1.0 Hz. During the AFM friction tests, the normal force gradually increased from 0 to 20 nN as the AFM tip approached, contacted, and compressed the GNC film surface. Lateral force was detected in noncontact, critical-contact, and full-contact states between the tip and film surfaces. This enabled the observation of nanofriction behavior for graphene edges in the critical-contact state and for the carbon film in the full-contact state. The detailed testing procedure is shown in Fig. 2(a). The lateral force was calibrated with a silicon grating (Mikromasch TGF11) by a wedge calibration method [31, 32]. The friction signal was acquired from the lateral force data in both the trace and retrace scans.

Figures 2(b)–2(d) illustrate the AFM friction signals of carbon films sliding against a silicon tip under the non-contact, critical-contact, and full-contact states, respectively. In the non-contact state, as the tip approached the film surface, the AFM friction signals were close to zero, with normal forces of 13, 14, 13, and 13 nN for the i–10, e+20, e+50, and e+80 samples, respectively, as shown in Fig. 2(b). Considering the AFM height images (Fig. S1(a) in the Electronic Supplementary Material (ESM)), both the undetected friction and height signals indicated that the tip did not contact the film surface. As the tip began to contact the film surface, the AFM friction signals (Fig. 2(c)), as well as the AFM height signals (Fig. S1(b) in the ESM), began to register, with normal forces of 14, 15, 14, and 14 nN for the i–10, e+20, e+50, and e+80 samples, respectively. In the critical-contact state, the tip just contacted and slid against the structural edges on the peak surface, reflecting the friction behavior of the graphene edges. Figure 2(c) shows that the a-C edge structure (i–10 sample) exhibited a high friction force (F_f) of 3.10 nN, while the GNC edge structures exhibited low F_f values of 3.21, 2.92, and 1.84 nN, corresponding to the e+20, e+50, and e+80 samples, respectively, indicating that the edges of the graphene nanocrystallites led to a decreasing friction force. Furthermore, as the tip completely contacted and compressed the film surface, the AFM friction signals are shown in Fig. 2(d), with a normal force of 20 nN. In the full-contact state, the tip compressed on the film surface, including the whole graphene and a-C structures. As shown in Fig. 2(d), the AFM friction signals revealed that the a-C film exhibited mild friction data with a low F_f of 3.75 nN, whereas the GNC films presented severe friction data with high friction forces. A comparison of the different GNC films revealed that as the edge states of the graphene nanocrystallites increased, the friction force decreased, with F_f values of 6.01, 5.07, and 3.86 nN for the e+20, e+50, and e+80 samples, respectively.

Based on the frictional results in the critical-contact state, when the edge structure transitioned from a-C to GNC, the graphene edges exhibited lower friction forces than the a-C edges, and the corresponding mechanism is illustrated in Fig. 3. When a critical normal load was applied on the tip–film sliding system, the tip surface contacted and slid over the morphological peaks of the carbon surface. Under this condition, the detected friction force originated solely from the edge structure of the peak surface terminals, disregarding the overall surface morphology. During this critical contact state, the actual interaction between Si and C atoms determined the edge friction behavior. As shown in Fig. 3, the contact between Si and C atoms at peak-surface terminals often involves dangling-bond interactions, which are considered the origin of the friction force. In a pure a-C system, the a-C edge structures primarily exposed the terminal sp^3 C atoms, and as the Si surface contacted those a-C edges, the sp^3 C atoms formed dangling bonds with the Si atoms, resulting in a high nanofriction force due to the dominant sp^3 C–Si interactions. In contrast, the GNC system, with its graphene nanocrystallites, created numerous high-density graphene edges, exposing abundant terminal sp^2 C atoms with dangling bonds in the atmosphere. As the tip surface contacted those graphene edges, the sp^2 C atoms interacted weakly with the Si atoms. This weaker sp^2 C–Si interaction, compared with sp^3 C–Si, contributed to the reduction in friction forces [33, 34]. Additionally, the edge and defect structures of graphene nanocrystallites can trap extra electrons due to the quantum well effect [35], reducing the potential of the contact edges and further lowering friction at the nanoscale, as suggested by simulation studies [36, 37]. Furthermore, the ordered arrangement of graphene edges on the top surface might also facilitate smoother tip–film sliding. Consequently, the high-density edges of the standing graphene nanocrystallites exhibited lower friction forces.

4 Graphene edge-regulated surface friction of GNC films

Next, the role of graphene edges in the surface friction of carbon films was investigated. Based on the frictional results under a normal force of 20 nN (Fig. 2(d)), the nanofriction behavior of the carbon surface was further tested under larger normal forces in the full-contact state. The tests were conducted under varying normal forces of 30, 40, 50, 60, and 70 nN, employing two applied modes: constant value mode and 4 μm-step varied value mode. Figures 4(a) and 4(b) show the friction image (lateral force) and the calculated friction curve of the GNC films in a 4 μm-step

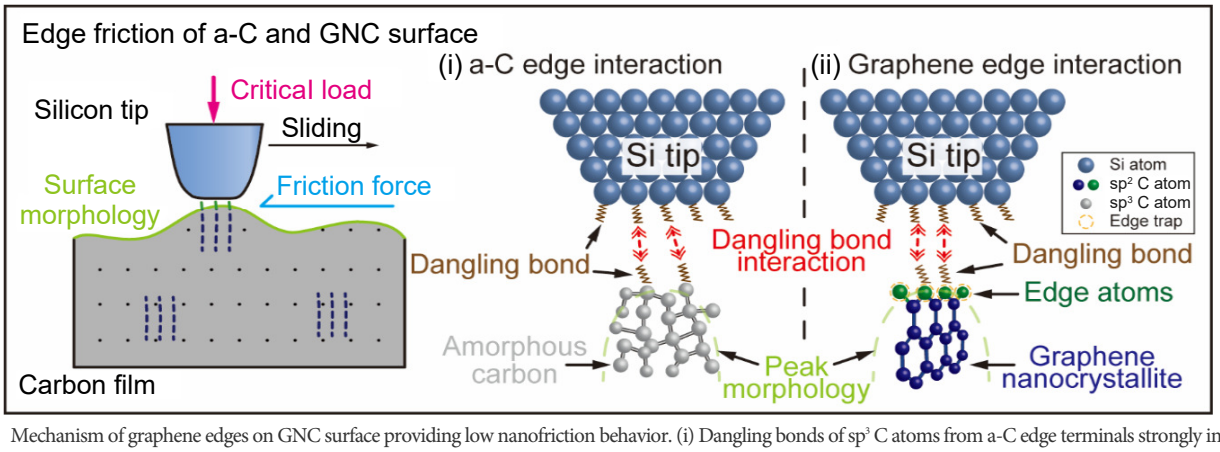

Fig. 3 Mechanism of graphene edges on GNC surface providing low nanofriction behavior. (i) Dangling bonds of sp^3 C atoms from a-C edge terminals strongly interact with Si atoms from tip surface; (ii) dangling bonds of sp^2 C atoms from high-density graphene edge terminals have weak interactions with Si atoms. Quantum wells at edges and defects trap extra electrons, reducing surface potential and resulting in a low contact interaction.

varied normal force mode. As the applied normal force was varied from 30 to 70 nN with an increment of 10 nN/4 μm, the nanofriction force at the tip–film interface presented an increasing trend with each step. Similar to the results shown in Fig. 2(d), the i–10 a-C film presented mild friction data, whereas the GNC films presented severe friction data. The fluctuation in the AFM friction data was proportional to the roughness of the surface. Figure 4(c) summarizes the calculated average friction force and friction coefficient with different normal forces in a constant value mode. The a-C film exhibited a low nanofriction force, with an average friction coefficient of 0.17±0.01. In contrast, the GNC film showed high nanofriction forces, with average friction coefficients of 0.26±0.09, 0.23±0.07, and 0.20±0.03 for the e+20, e+50, and e+80 samples, respectively.

Based on the above frictional results in the full-contact state, the surface friction force of the GNC films tended to decrease as the density of the graphene nanocrystallite edges increased, and the underlying mechanism is discussed in Fig. 5. During the full contact state, all the atoms at the contact point contributed to the surface friction force. As illustrated in Fig. 5, a 16-nm-diameter tip made contact with the carbon surface, where both sp^2 and sp^3 C atoms interacted with Si atoms at the contact point. The proportion of these atoms determined the surface friction force. According to the frictional results of edge structures, the sp^2 C atoms from graphene edges could provide a weaker dangling-bond interaction with Si atoms than the stronger interaction from the sp^3 C atoms in the a-C structure. Thus, the density of the graphene nanocrystallite edges directly influenced the surface friction force of the GNC film: higher graphene edge density resulted in a lower surface friction force. However, the GNC film exhibited a greater surface friction force than the a-C film, which seemed inconsistent with the edge friction force. This discrepancy could be attributed to the surface morphology. The GNC films had far rougher surfaces than the a-C film (see the AFM height image in Fig. S1 in the ESM), contributing to a greater surface friction force. Therefore, the high-density edges of the graphene nanocrystallites in the GNC film effectively controlled the nanofriction behavior of the carbon surface.

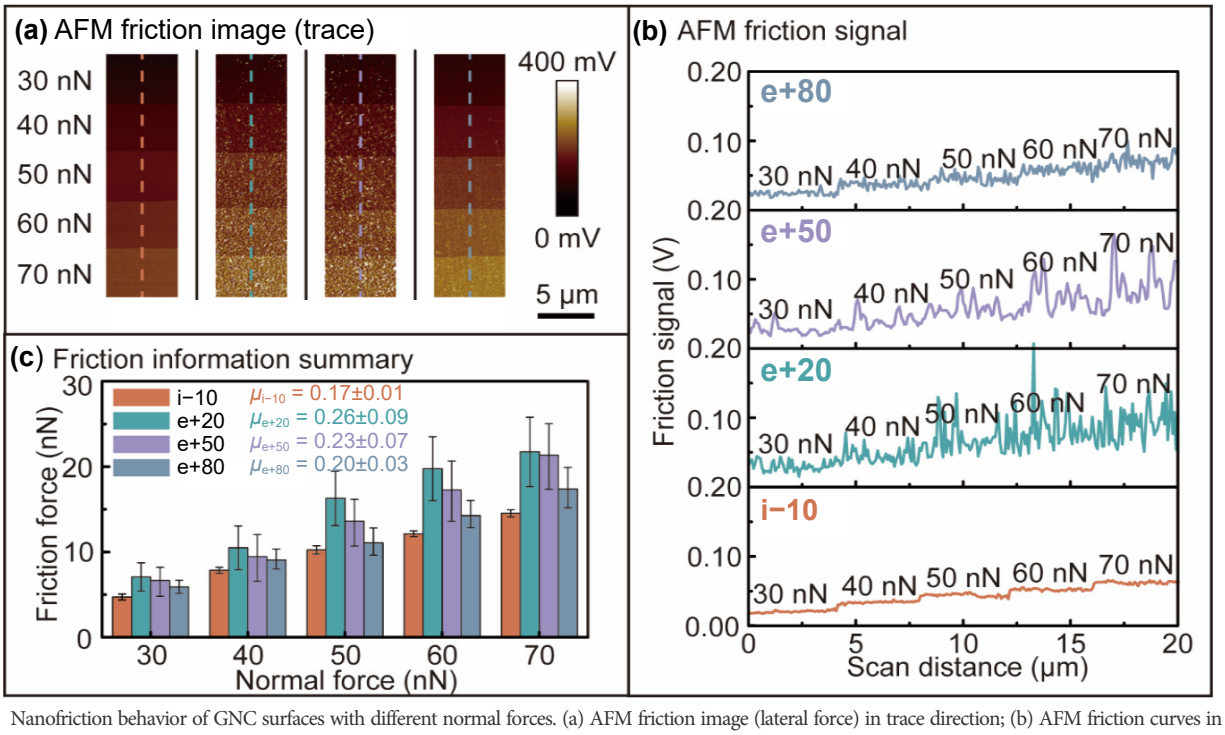

Fig. 4 Nanofriction behavior of GNC surfaces with different normal forces. (a) AFM friction image (lateral force) in trace direction; (b) AFM friction curves in trace direction; (c) typical results of friction force vs. normal force.

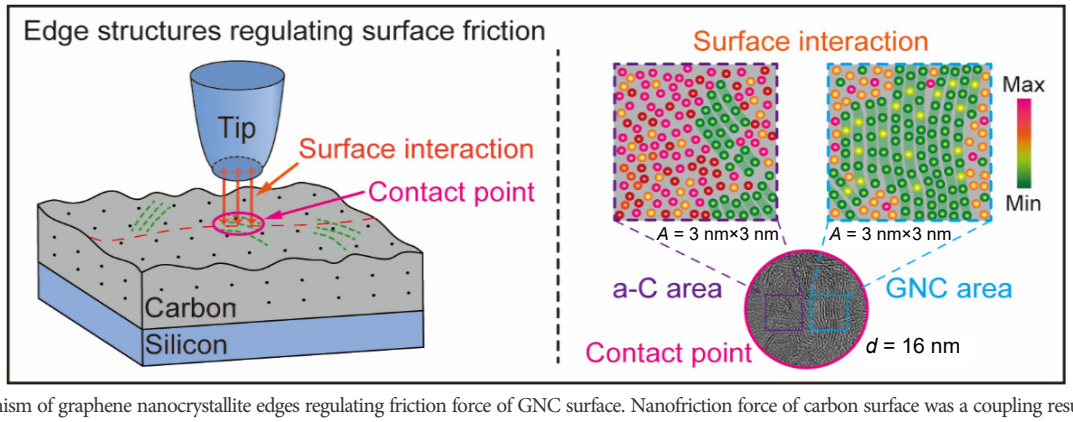

Fig. 5 Mechanism of graphene nanocrystallite edges regulating friction force of GNC surface. Nanofriction force of carbon surface was a coupling result of dangling-bond interaction of sp^2 C and sp^3 C atoms, which originated from graphene and amorphous structure edges. High density of graphene edges provided more sp^2 C atoms for lowering the friction force.

5 Conclusions

In conclusion, to explore the friction behavior of graphene edges within a carbon surface, pure carbon films with surface structures ranging from amorphous to nanocrystalline graphene were fabricated in an ECR plasma system. The GNC film structure featured vertically growing graphene nanocrystallites implanted in the a-C phase, with high-density edges exposed on the top surface. The edge and surface friction behaviors of the GNC film sliding against the AFM Si tip were investigated under the critical-contact and full-contact states, respectively, revealing the nature of the graphene edges and their roles in regulating the friction behavior of the carbon surface. The conclusions are summarized as follows: (1) Graphene edges exhibit lower friction forces than a-C edges. (2) The friction behavior of the carbon surface can be adjusted by graphene edges: The more edges of the graphene nanocrystallite, the lower the nanofriction force of the carbon surface. (3) The mechanism of regulating friction behavior involves the edges of graphene nanocrystallites providing plentiful sp^2 C atoms that form dangling bonds with Si atoms through weak bonding interactions and controlling the surface potential, thereby lowering the nanofriction force. This work is essential for the development of graphene and its related structural edges in the structural design and nanofriction applications of carbon films.

Acknowledgements

The authors would like to thank the National Natural Science Foundation of China (Nos. 52105169 and 52105170) for their financial support. The authors would like to thank the Beijing Natural Science Foundation (No. 2222048) for financial support. The authors wish to acknowledge the assistance on FIB and TEM received from the Electron Microscope Center of Shenzhen University.

Availability of data and materials

The data that support the findings of this study are available from the corresponding author upon reasonable request.

Declaration of competing interest

The authors have no competing interests to declare that are relevant to the content of this article. The author Dongfeng Diao is the Editorial Board member of this journal.

Electronic Supplementary Material

Supplementary material is available in the online version of this article at https://doi.org/10.26599/FRICT.2025.9441086.

References

[1] Soto F, Wang J, Ahmed R, Demirci U. Medical micro/nanorobots in precision medicine. *Adv Sci* **7**(21): 2002203 (2020)
[2] Imboden M, Han H, Chang J, Pardo F, Bolle C A, Lowell E, Bishop D J. Atomic calligraphy: The direct writing of nanoscale structures using a microelectromechanical system. *Nano Lett* **13**(7): 3379–3384 (2013)
[3] Wang Y Q, Zhang C J, Meng X L, Zhang Q S, Li H Y, Chen F, Yang Q, Zhang W Q, Zheng Y J, Chen S C. Quantitative and real-time evaluation of pressure on brain spatula with wireless and compact sensing system. *Adv Funct Mater* **33**(9): 2210596 (2023)
[4] Hod O, Meyer E, Zheng Q S, Urbakh M. Structural superlubricity and ultralow friction across the length scales. *Nature* **563**(7732): 485–492 (2018)
[5] Huang Y H, Sai Sarathi Vasan A, Doraiswami R, Osterman M, Pecht M. MEMS reliability review. *IEEE T Device Mat Re* **12**(2): 482–493 (2012)
[6] Li X D, Bhushan B. Micromechanical and tribological characterization of hard amorphous carbon coatings as thin as 5 nm for magnetic recording heads. *Wear* **220**(1): 51–58 (1998)
[7] Spear J C, Ewers B W, Batteas J D. 2D-nanomaterials for controlling friction and wear at interfaces. *Nano Today* **10**(3): 301–314 (2015)
[8] Lu Y M, Wang Y L, Huo F, Chen W, Ma M, Ding W L, He H Y, Zhang S J. Ultralow friction and high robustness of monolayer ionic liquids. *ACS Nano* **16**(10): 16471–16480 (2022)
[9] Yu K M, Zou K, Lang H J, Peng Y T. Nanofriction characteristics of h-BN with electric field induced electrostatic interaction. *Friction* **9**(6): 1492–1503 (2021)
[10] Mo Y F, Turner K T, Szlufarska I. Friction laws at the nanoscale. *Nature* **457**(7233): 1116–1119 (2009)
[11] DelRio F W, de Boer M P, Knapp J A, David Reedy E Jr, Clews P J, Dunn M L. The role of van der Waals forces in adhesion of micromachined surfaces. *Nat Mater* **4**(8): 629–634 (2005)
[12] Sankar K M, Kakkar D, Dubey S, Garimella S V, Goyat M S, Joshi S K, Pandey J K. Theoretical and computational studies on nanofriction: A review. *P I Mech Eng J—J Eng* **234**(3): 448–465 (2003)
[13] Pierno M, Bruschi L, Fois G, Mistura G, Boragno C, de Mongeot F B, Valbusa U. Nanofriction of neon films on superconducting lead. *Phys Rev Lett* **105**: 016102 (2010)
[14] Liu H Z, Zong W J, Cheng X. Load- and size effects of the diamond friction coefficient at the nanoscale. *Tribol Lett* **68**(4): 120 (2020)
[15] Ge X Y, Chai Z Y, Shi Q Y, Liu Y F, Wang W Z. Graphene superlubricity: A review. *Friction* **11**(11): 1953–1973 (2023)
[16] Greenwood G, Kim J M, Nahid S M, Lee Y, Hajarian A, Nam S, Espinosa-Marzal R M. Dynamically tuning friction at the graphene interface using the field effect. *Nat Commun* **14**: 5801 (2023)
[17] Vilhena J G, Pimentel C, Pedraz P, Luo F, Serena P A, Pina C M, Gnecco E, Pérez R. Atomic-scale sliding friction on graphene in water. *ACS Nano* **10**(4): 4288–4293 (2016)
[18] Li S Z, Li Q Y, Carpick R W, Gumbsch P, Liu X Z, Ding X D, Sun J, Li J. The evolving quality of frictional contact with graphene. *Nature* **539**(7630): 541–545 (2016)
[19] Peng Y T, Zeng X Z, Yu K, Lang H J. Deformation induced atomic-scale frictional characteristics of atomically thin two-dimensional materials. *Carbon* **163**: 186–196 (2020)
[20] Wang W, Zhang Y, Li Z H, Qian L M. Controllable friction on graphene via adjustable interfacial contact quality. *Adv Sci* **10**(30): 2303013 (2023)
[21] Kwon S, Ko J H, Jeon K J, Kim Y H, Park J Y. Enhanced nanoscale friction on fluorinated graphene. *Nano Lett* **12**(12): 6043–6048 (2012)
[22] Abergel D S L, Apalkov V, Berashevich J, Ziegler K, Chakraborty T. Properties of graphene: A theoretical perspective. *Adv Phys* **59**(4): 261–482 (2010)
[23] Ge L, Liu Q, Jiang D, Ding L J, Wen Z R, Guo Y S, Ding C F, Wang K. Oxygen vacancy enhanced photoelectrochemical performance of Bi_2MoO_6/B, N co-doped graphene for fabricating lincomycin aptasensor. *Biosens Bioelectron* **135**: 145–152 (2019)
[24] Fu L, Zhang K Y, Zhang W L, Chen J, Deng Y, Du Y W, Tang N J. Synthesis and intrinsic magnetism of bilayer graphene nanoribbons. *Carbon* **143**: 1–7 (2019)
[25] Sun K, Fan X, Yang L, Chen S C, Fan J W, Diao D F. Graphene nanocrystallites induced short run-in period with low electric power at current-carrying sliding interface. *Appl Surf Sci* **568**: 150902 (2021)
[26] Yin Z Y, Yu Y F, Chen H, Li J H, Bai L C. Nanofriction behaviors between silicon-doped diamond-like carbon films under different testing conditions. *Comp Mater Sci* **188**: 110182 (2021)
[27] Wang W, Huang X, Huang Y Q, Wang Y. Nanoscale friction of tetrahedral amorphous diamond-like carbon film after thermal annealing. *Tribol Int* **190**: 109064 (2023)
[28] Komlenok M S, Kononenko V V, Zavedeev E V, Frolov V D, Arutyunyan N R, Chouprik A A, Baturin A S, Scheibe H J, Shupegin M L, Pimenov S M. Laser surface graphitization to control friction of diamond-like carbon coatings. *Appl Phys A—Mater* **121**(3): 1031–1038 (2015)
[29] Ferrari A C, Robertson J. Resonant Raman spectroscopy of disordered, amorphous, and diamondlike carbon. *Phys Rev B* **64**(7): 075414 (2001)
[30] Ferrari A C, Meyer J C, Scardaci V, Casiraghi C, Lazzeri M, Mauri F,

Piscanec S, Jiang D, Novoselov K S, Roth S, et al. Raman spectrum of graphene and graphene layers. *Phys Rev Lett* **97**(18): 187401 (2006)
[31] Varenberg M, Etsion I, Halperin G. An improved wedge calibration method for lateral force in atomic force microscopy. *Rev Sci Instrum* **74**(7): 3362–3367 (2003)
[32] Yang L, Qi K, Diao D F, Wang P F, Xue P D. Magnetostrictive friction of graphene sheets embedded carbon film. *Carbon* **159**: 617–624 (2020)
[33] Li Q Y, Tullis T E, Goldsby D, Carpick R W. Frictional ageing from interfacial bonding and the origins of rate and state friction. *Nature* **480**(7376): 233–236 (2011)
[34] Wang J J, Li L, Wang J D, Yang W T, Guo P, Li M, Liu D D, Zeng H X, Zhao B. First-principles study on the nanofriction properties of diamane: The thinnest diamond film. *Nanomaterials* **12**(17): 2939 (2022)
[35] Zhang X, Wang C, Sun C Q, Diao D F. Magnetism induced by excess electrons trapped at diamagnetic edge-quantum well in multi-layer graphene. *Appl Phys Lett* **105**(4): 042402 (2014)
[36] Wang J J, Li M, Zhang X H, Cai X L, Yang L F, Li J M, Jia Y. An atomic scale study of ultralow friction between phosphorus-doped nanocrystalline diamond films. *Tribol Int* **86**: 85–90 (2015)
[37] Wang W, Shen J, He Q C. Microscale superlubricity of graphite under various twist angles. *Phys Rev B* **99**(5): 054103 (2019)

Kun Sun received his Ph.D. degree in mechanical engineering from Xi'an Jiaotong University, Xi'an, China, in 2020. He is currently an associate professor at the College of Mechanical and Energy Engineering, Beijing University of Technology, Beijing, China. His research is focused on nanosurface engineering and tribology. He is interested in the multiscale tribological properties of the carbon material, as well as current-carrying tribology.

Ri Pan received his Ph. D. degree in mechanical engineering from Xiamen University, Xiamen, China, in 2014. He is working as an associate professor at the Beijing University of Technology, Beijing, China. His research interests include precision machining equipment and technology.

Meijie Yin completed her doctoral studies at Hunan University, Changsha, China. She is currently working at the Electron Microscope Center at Shenzhen University, Shenzhen, China, and is conducting research on materials characterization. Her work primarily involves the characterization of material microstructures, with a particular emphasis on the application of advanced transmission electron microscopy techniques in exploring the intricate relationships between microstructure and material behavior.

Dongfeng Diao obtained his Ph.D. degree in mechanical engineering from Tohoku University, Sendai, Japan, in 1992. He is currently a distinguished professor and director for the Institute of Nanosurface Science and Engineering (INSE) and the Electron Microscope Center (EMC) at Shenzhen University, Shenzhen, China. He is a foreign member of the Engineering Academy of Japan (EAJ). His research interests include nanosurface science and technology, ECR-based quantum manufacturing, quantum superlubricity, and sensing technology.